Dramatic enhancement of near-infrared intersubband absorption in c-plane AlInN/GaN superlattices

M. Shirazi-HD, K. Turkmeneli, S. Liu, S. Dai, C. Edmunds, J. Shao, G. Gardner, D. N. Zakharov, M. J. Manfra, and O. Malis

Citation: Applied Physics Letters **108**, 121108 (2016); doi: 10.1063/1.4944847
View online: http://dx.doi.org/10.1063/1.4944847
View Table of Contents: http://scitation.aip.org/content/aip/journal/apl/108/12?ver=pdfcov
Published by the AIP Publishing

Dramatic enhancement of near-infrared intersubband absorption in c-plane AlInN/GaN superlattices

M. Shirazi-HD,[1,2] K. Turkmeneli,[3] S. Liu,[1] S. Dai,[3] C. Edmunds,[3] J. Shao,[2,3] G. Gardner,[2,4] D. N. Zakharov,[5] M. J. Manfra,[1,2,3,4] and O. Malis[3,a)]
[1]*School of Electrical and Computer Engineering, Purdue University, West Lafayette, Indiana 47907, USA*
[2]*Birck Nanotechnology Center, West Lafayette, Indiana 47907, USA*
[3]*Department of Physics and Astronomy, Purdue University, West Lafayette, Indiana 47907, USA*
[4]*School of Materials Engineering, Purdue University, West Lafayette, Indiana 47907, USA*
[5]*Center for Functional Nanomaterials, Brookhaven National Laboratory, Upton, New York 11973, USA*

(Received 6 January 2016; accepted 15 March 2016; published online 24 March 2016)

We report substantial improvement of near-infrared (2–2.6 μm) intersubband absorption in c-plane AlInN/GaN superlattices grown by molecular beam epitaxy. Progress was obtained through optimization of AlInN growth conditions using an AlInN growth rate of 0.9-nm/min at substrate temperature of 550 °C, as well as by judiciously placing the charge into two delta-doping sheets. Structural characterization suggests that AlInN crystal quality is enhanced and interface roughness is reduced. Importantly, near-infrared absorption data indicate that the optical quality of the AlInN/GaN superlattices is now comparable with that of AlN/GaN superlattices designed to exploit near-infrared intersubband transitions. © *2016 AIP Publishing LLC*. [http://dx.doi.org/10.1063/1.4944847]

III-nitride semiconductors are currently intensively studied for applications in infrared optoelectronics,[1–3] such as detectors and emitters for spectral regions not easily accessible with other semiconductors. Near-infrared light detection and modulation have been successfully demonstrated using nitride quantum wells (QWs) and dots. However, near-infrared emission from III-nitride devices proved harder to achieve. One prime reason for the lag of near-infrared lasers is the considerable lattice-mismatch between GaN and the high-Al composition $Al_xGa_{1-x}N$ ($x > 0.5$) necessary for laser operation in the near-infrared. This mismatch limits the thickness of the heterostructures that can be grown before macroscopic defects such as cracks are generated.[4] To overcome this challenge, we investigate near-lattice-matched c-plane AlInN/GaN superlattices. $Al_{0.83}In_{0.17}N$ is exactly lattice-matched to GaN in the c-plane,[1] and therefore thick AlInN/GaN structures can be grown along the c-direction. Near-infrared intersubband absorption (ISBA) in AlInN/GaN superlattices has so far been demonstrated in materials grown by MOCVD[1] and molecular beam epitaxy (MBE).[5–8] Since ISBA is the optical property most relevant for infrared devices, these reports were promising for near-infrared devices. However, the initial results also highlighted the challenges of high quality AlInN growth. ISBA is extremely sensitive to nanoscale structural imperfections such as interface roughness and alloy non-uniformity. The first detailed structural studies of thick $Al_{0.83}In_{0.17}N$ layers[8–10] and AlInN/GaN superlattices showed inhomogeneous alloy composition consisting of In-rich columns along the growth direction. Our detailed quantitative comparison of c-plane AlGaN/GaN and AlInN/GaN superlattices revealed that the latter exhibit considerably lower ISBA and broader spectra than expected theoretically or measured in AlGaN/GaN.[8] The inferior ISBA of AlInN/GaN superlattices was attributed primarily to columnar alloy inhomogeneity in the AlInN barriers that depletes the charge from the quantum wells.[8] Here, we report dramatic enhancement of near-infrared ISBA in AlInN/GaN superlattices that was achieved through optimization of the MBE growth conditions and silicon doping profile.

AlInN heterostructures were grown by plasma-assisted MBE on low-defect semi-insulating c-plane GaN templates on sapphire. Table I summarizes the parameters of the samples discussed here. Active nitrogen was supplied by a radio-frequency plasma source with a power of 300 W and 0.5 SCCM for AlN/GaN, and 400 W and 0.5 SCCM for AlInN/GaN resulting in GaN growth rates of 8.6 and 9.6-nm/min under nitrogen-limited growth, respectively. Growth of AlInN films requires a different approach to that typical of AlGaN MBE since indium desorption limits the allowable growth temperature.[8] Unlike aluminum, indium incorporation depends sensitively on substrate temperature T_s in the range $500\,°C < T_s < 600\,°C$. While increasing the substrate temperature does, in general, enhance adatom surface mobility, it can also significantly reduce indium incorporation.[11] We found the maximum temperature at which we could reliably produce thick $Al_{0.83}In_{0.17}N$ films to be 550 °C as measured by optical pyrometry calibrated to the melting point of aluminum (660 °C). Thus, our strategy was to grow the superlattices at the highest temperature possible consistent with controlled indium incorporation. Optimum growth conditions were obtained with an In/Al flux ratio of 0.9 and a growth rate of 0.9-nm/min for AlInN under nitrogen-rich conditions. These conditions are a substantial departure from our previously reported work in which the substrate was maintained at $T \leq 530\,°C$ and the AlInN growth was 3.3 nm/min.[8] We speculate that the reduced growth rate allows adatoms more time to explore the growth front before incorporation, and increasing the growth temperature from 530 °C to 550 °C enhances adatom mobility. Both processes enhance crystal quality and reduce lateral inhomogeneity.[12,13] A more complete discussion of the relation between

a)Author to whom correspondence should be addressed. Electronic mail: omalis@purdue.edu.

TABLE I. Structural parameters, doping profile, growth conditions, and the results of the near-infrared ISBA measurements for the samples discussed in this study. Layer thicknesses were obtained from HRXRD and confirmed by TEM, while the doping densities were calibrated in GaN with SIMS. The experimental results for ISBA for the ground to first excited state transition (E1–E2), i.e., transition energy, full-width at half maximum (FWHM), and integrated absorbance, are compared with the corresponding calculated values. The location of the δ-doping is given in parenthesis in nm from the beginning of growth of the QW.

Sample	Superlattice parameters (well/barrier nm)	Barrier material	Cont. doping (well/barrier cm^{-3})	Delta doping (cm^{-2}) (Position in QW)	Gr. temp. Well gr. rate Barrier gr. rate	Energy (meV)		Int. Abs (meV)		FWHM (meV)
						Expt.	Calc	Expt.	Calc	Expt.
H[8]	20 × 3.5/2.5	$Al_{0.84}In_{0.16}N$	5.9×10^{19}/ 1.4×10^{20}	2.7×10^{14} (1.8 nm)	530 °C 7 nm/min 3.3 nm/min	665	485	6	113	211
I	15 × 4.6/1.5	$Al_{0.89}In_{0.11}N$	7×10^{19}/ 3.1×10^{20}	2.9×10^{14} (2.3 nm)	530 °C 7 nm/min 1.6 nm/min	578	533	33	113	136
J	15 × 3.5/2.8	$Al_{0.90}In_{0.10}N$	7×10^{19}/ 5.4×10^{20}	2.9×10^{14} (1.75 nm)	550 °C 7 nm/min 0.9 nm/min	567	580	52	121	150
K	15 × 4.1/2.5	$Al_{0.87}In_{0.13}N$	0/0	1.5×10^{14}, 1.5×10^{14} (1.4 nm, 2.7 nm)	550 °C 9.6 nm/min 0.9 nm/min	528	444	54	58	128
L	15 × 4.3/2.5	$Al_{0.89}In_{0.11}N$	5.1×10^{19}/ 5.4×10^{20}	1.5×10^{14} (1.4 nm)	550 °C 9.6 nm/min 0.9 nm/min	469	532	88	98	144
M	15 × 4.4/2.5	$Al_{0.89}In_{0.11}N$	5.1×10^{19}/ 5.4×10^{20}	1.5×10^{14}, 1.5×10^{14} (1.5 nm, 2.9 nm)	550 °C 9.6 nm/min 0.9 nm/min	545	508	209	88	126
N	15 × 5.9/2.8	AlN	5.6×10^{19}/ 5.6×10^{19}	1.5×10^{14}, 1.5×10^{14} (2 nm, 3.9 nm)	720 °C 8.8 nm/min 8.8 nm/min	614	620	234	128	156

growth conditions and the structural properties of these films is beyond the scope of this letter and will be presented in a forthcoming publication.

The growth sequence consists of a high temperature (720 °C) GaN buffer layer, a growth pause to cool the sample to the target AlInN growth temperature, the 15 QW AlInN/GaN superlattice, and finally a 7.5-nm GaN capping layer. The bulk Si-doping level in GaN grown at 7-nm/min was calibrated using secondary ion mass spectrometry (SIMS) to be $7 \times 10^{19}\,cm^{-3}$. The AlInN Si-doping density was estimated by taking the Si incorporation rate in GaN from SIMS and adjusting for the difference in growth rates. To further increase charge density, δ-doping was deposited during a growth pause in the GaN well as indicated in Table I. During this pause, the Ga, Al, and In shutters were closed.

The AlInN/GaN superlattices were characterized *in-situ* with reflection high-energy electron diffraction (RHEED), *ex-situ* with atomic-force microscopy (AFM), and high-resolution x-ray diffraction (HRXRD). Theoretical simulation of the HRXRD using the Panalytical X'PERT-EPITAXY package combined with transmission electron microscopy (TEM) imaging of a few representative samples allowed for the determination of the well and barrier thicknesses, and the Al-composition.

Fig. 1 compares the properties of an AlInN/GaN superlattice grown at 550 °C and AlInN growth rate 0.9 nm/min showing strong ISBA with a superlattice grown at 530 °C combined with an elevated AlInN growth rate of 3.3 nm/min under conditions similar to sample H.[8] Lower temperature ($T_s \leq 530$ °C) and higher growth rate ($\geq$3 nm/min) AlInN barriers consistently result in weak and broad infrared absorption features when compared to superlattices grown at higher temperature (550 °C) and lower AlInN growth rate (0.9 nm/min). As seen in Fig. 1(a), elevated substrate temperature improves the surface morphology, reducing the RMS roughness over 1 μm × 1 μm from 3.1 nm to 0.67 nm. This change in morphology is reflected in the RHEED pattern (Fig. 1(b)) observed at the end of each growth. While the RHEED remains streaky throughout the higher temperature growth (indicative of quasi-2D growth), the RHEED rapidly develops into truncated spots during lower temperature growth indicating a transition to a 3D growth mode. Finally, the HRXRD $\omega/2\Theta$ scans demonstrate the difference in structural quality. The 550 °C and 0.9 nm/min growth yields strong superlattice satellite peaks and Pendellösung fringes, while for 530 °C and 3.3 nm/min growth, these features are greatly diminished. The impact of these changes to growth conditions on infrared absorption, the focus of this work, is discussed below.

The optical properties of the AlInN/GaN superlattices were characterized using Fourier-transform infrared spectroscopy at room-temperature on samples polished into 45° multipass waveguides. All spectra display the normalized absorbance obtained from transmission spectra.[8] The electric-field overlap was estimated for each sample (0.38–0.56) by calculating the average electric-field value over the active region at the peak absorption wavelength, assuming a node at the air-semiconductor interface. The experimental results are summarized in Table I and Fig. 2. The experimental integrated intensity in Table I was obtained by numerically integrating the absorbance curve over the available experimental range.

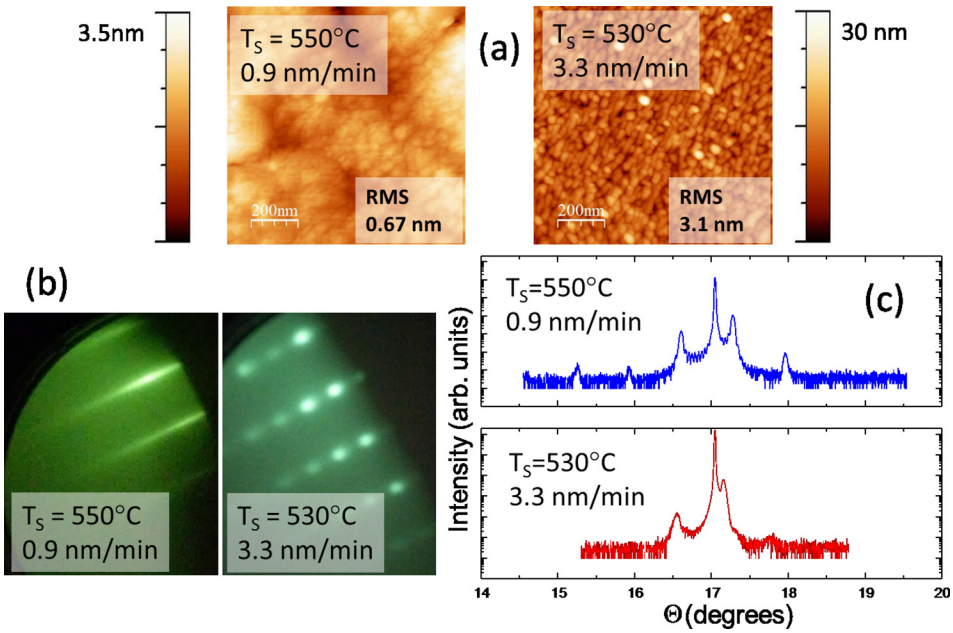

FIG. 1. (a) AFM of superlattice grown at 550 °C and 0.9 nm/min (left) and 530 °C and 3.3 nm/min (right). (b) RHEED pattern (left: 550 °C and 0.9 nm/min, right: 530 °C and 3.3 nm/min) observed at the termination of superlattice growth. (c) HRXRD of superlattices demonstrating sharp satellite peaks and Pendellösung fringes for 550 °C and 0.9 nm/min and greatly diminished satellite peaks and absence of Pendellösung fringes for 530 °C and 3.3 nm/min.

The band structures of the AlInN/GaN superlattices were calculated self-consistently using an eight-band **k·p** model with the **nextnano3** software.[14] Si-doping is considered to be thermally ionized with an activation energy of 15 meV in GaN and 100 meV in AlInN.[15] Many-body corrections to the transition energies were calculated according to Ref. 16. The details of the calculation for the integrated intensity are given in Ref. 8.

Previously, we investigated the effect of AlInN inhomogeneity on the 3D band structure and ISBA of AlInN/GaN superlattices[8] using experimental information available at the time from the literature.[10] Atom probe tomography had found large in-plane variation of the indium composition (5%–40%) with the highest In composition occurring at the meeting points of honeycomb walls.[10] The AlInN columnar structure was modeled with nanorods of radially decreasing In-composition oriented along the growth direction. We found the inclusion of the nanorods to distort the 3D band structure leading to localization of charge carriers in the nanorods and charge density reduction in the QWs.[8] This explains the lower than expected experimental QW ISBA.

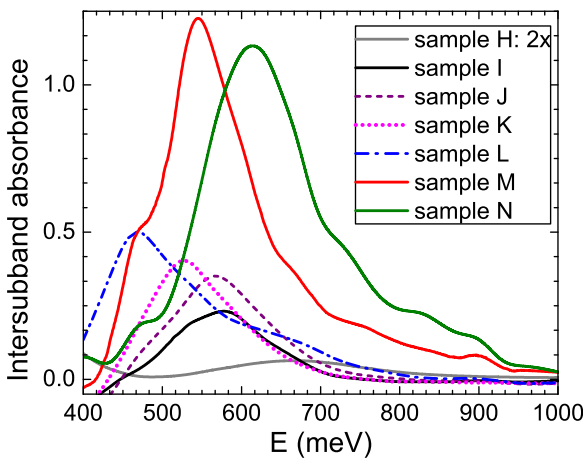

FIG. 2. Summary of near-infrared intersubband absorbance spectra corresponding to samples I–N from Table I.

Moreover, the QW ISBA is blue-shifted likely due to higher-than-average Al-content (95%) in the barrier regions surrounding the In-rich nanorods.

Here, we show that growth rate and temperature have a strong effect on the amplitude of the ISBA and structural properties of AlInN/GaN superlattices. Sample H in Table I is representative of absorption spectra measured on samples grown at lower temperature (530 °C) with an AlInN growth rate of 3.3 nm/min and was reproduced from Ref. 8 for comparison (peak absorbance of sample H was approximately 0.1). Lowering the AlInN growth rate has a positive effect on the alloy uniformity as first demonstrated by Kaun *et al.*[12] Sample I was obtained with an AlInN growth rate of 1.6-nm/min, lower than the value 3.3 nm/min used in our previous work, but at the same growth temperature of 530 °C. The corresponding absorption peaks at 578 meV, in better agreement with the calculated value of 533 meV than our previous data (see sample H). Moreover, the FWHM is substantially lower than previously reported (136 meV vs. 211 meV), which is indicative of reduced interface and alloy scattering. Since we attributed the large discrepancy between theoretical and experimental peak energy of sample H to inhomogeneous barrier composition, we suggest the decrease of the blue shift to be significant and indicative of improved barrier alloy uniformity. Furthermore, the integrated intensity is more than a factor of 5 larger for sample I than for sample H. This increase cannot be explained by the increase in Si-doping alone but must also be due to improved charge confinement associated with better barrier alloy uniformity. While sample I is a substantial improvement over sample H, its integrated absorption is still considerably lower than predicted theoretically.

By increasing the growth temperature from 530 to 550 °C, and further reducing the AlInN growth rate to 0.9-nm/min, we were able to additionally increase the near-infrared integrated absorption. Sample J is representative of the ISBA corresponding to these growth conditions. While increase in integrated ISBA in this case may be, in part, due to larger doping level in the barrier as a consequence of

lower growth rate, the enhanced barrier doping alone cannot quantitatively account for observed behavior. Again the optical data imply improved epilayer quality stems from growth rate reduction.

Dopant profile also plays a major role in determining the infrared optical properties of AlInN/GaN multi-quantum wells. Previously, we could observe AlInN/GaN ISBA directly only at very high doping levels that we achieved through heavy Si δ-doping in the QWs. This suggests that Si activation in AlInN is considerably lower than expected theoretically, corroborating recent observations made with other experimental techniques.[17,18] Although band structure calculations indicate that all Si in the barriers should be activated, in the past we were not able to measure ISBA in AlInN/GaN superlattices unless we added Si δ-doping in the QWs. This is in stark contrast with measurements of Al(Ga)N/GaN superlattices. Also in sharp contrast with findings for AlGaN/GaN, δ-doping of AlInN/GaN superlattices at the end of the QW resulted in low or absent near-infrared absorption as compared to the samples δ-doped inside the QW. This is additional evidence for lower than expected Si activation in AlInN. In this case, unintentional Si dopant incorporation into the barrier may reduce the efficacy of doping. It is also possible that δ-doping at the end of the well results in higher interface roughness in AlInN/GaN superlattices as compared to AlGaN/GaN. Roughening induced by extreme Si-doping has been documented in other studies,[19] but so far, we have no evidence of additional Si-induced interface roughening.

As a consequence of lower than expected barrier dopant activation, AlInN/GaN ISBA is extremely sensitive to the level and location of the well δ-doping. Due to the field-induced band distortion (see inset of Fig. 3), not all well Si is activated. Moreover, Si activation decreases with increasing distance from the left QW edge. Sample K was doped using only two δ-doping layers located at one third and two-thirds of the well width from the interfaces. This sample exhibited absorption similar to sample J, but that is in better agreement with theoretical integrated absorption. The peak energy difference between measurements and calculation may, in this case, be due to experimental uncertainties in establishing the exact structural parameters of the real sample.

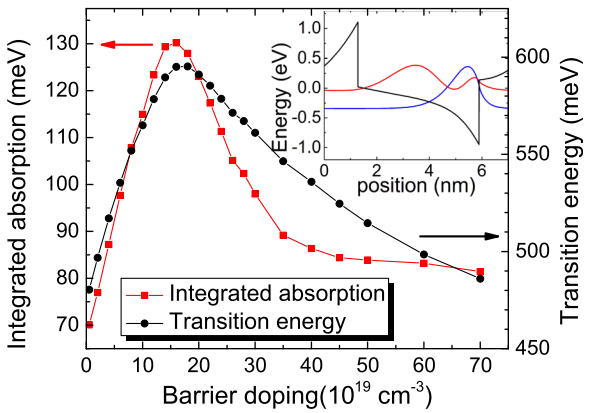

FIG. 3. Calculated transition energy and integrated absorbance for sample M as a function of barrier doping level. The well doping is maintained at the nominal level indicated in Table I. Inset: Conduction band and wavefunctions for the ground and first excited states of a AlInN/GaN superlattices with the structure of sample M, and Si-doping corresponding to the peaks in the main panel (barrier: $1.6 \times 10^{20}\,\mathrm{cm}^{-3}$, well: $5.6 \times 10^{19}\,\mathrm{cm}^{-3}$, and 2 δ-doping sheets of $1.5 \times 10^{14}\,\mathrm{cm}^{-2}$ located at 1/3 and 2/3 of the well width). The Fermi level corresponds to the zero of the y-axis in the inset.

Samples L and M further support the importance of well δ-doping distribution on ISBA. In addition to uniform well and barrier doping, sample L had a δ-doping sheet located at one-third of the QW width from the left QW edge, while sample M had 2 δ-doping layers located at one third and two-thirds of the well width from the interfaces (same as sample K). The integrated absorption of sample L is also in quantitative agreement with theoretical calculations. Most interestingly, however, sample M exhibits improvement of the ISBA integrated intensity beyond naïve theoretical expectations.

Since we have higher confidence in the determination of the structural parameters and dopant activation in GaN, to shed light on ISBA of sample M, we focused on the effect of the barrier doping activation on ISBA. Fig. 3 shows the theoretical dependence of the transition energy and integrated intensity on barrier doping when the well is kept at the nominal level (Table I). Both curves exhibit peaks for barrier doping around $1.6 \times 10^{20}\,\mathrm{cm}^{-3}$. The initial increase of the integrated intensity and transition energy with charge density are easily understood from the definition of ISBA, and many-body effects, respectively. Past the peak, the transition energy and integrated intensity decrease due to flattening of the conduction band profile and resulting oscillator strength decrease, respectively (see inset of Fig. 3). Sample M transition energy (545 meV) can only be explained if we assume lower activation of the barrier Si than expected theoretically. The plot suggests that the net activated barrier charge density is either $3.5 \times 10^{20}\,\mathrm{cm}^{-3}$ or $7 \times 10^{19}\,\mathrm{cm}^{-3}$ (as opposed to $5.4 \times 10^{20}\,\mathrm{cm}^{-3}$ expected theoretically). Given all our optical results, we believe that the lower number ($\sim$13% of nominal value) is more representative of the charge activated from AlInN. Surprisingly, Fig. 3 also shows that the peak theoretical integrated intensity value (130 meV) is significantly lower than the measured value (209 meV). We believe this to be a limitation of our theoretical model that applies to the case when the Fermi level is above the first excited state (samples L–N). More sophisticated theoretical treatments including multi-plasmon effects[20] may be necessary to accurately describe the behavior of these highly doped samples.

The ISBA in AlInN/GaN QWs was compared to that of similar AlN/GaN QWs (sample N) grown under optimal conditions for this material combination (substrate temperature 720 °C and group III-rich conditions). We found good agreement between experimental results and theoretical calculations for the transition energy of sample N. The ISBA linewidth of sample N is comparable to that of sample M, suggesting similar structural quality. It is important to note that the integrated intensities of samples M and N are in quantitative agreement with each other, but larger than predicted theoretically, likely due to the reasons discussed above.

In conclusion, we were able to drastically enhance intersubband absorption in AlInN/GaN superlattices by optimizing AlInN growth conditions. The integrated absorption was

increased more than an order of magnitude by reducing the AlInN growth rate to 0.9-nm/min, increasing the growth temperature to 550 °C, and placing Si into two δ-doping sheets. These optical results are consistent with reduced alloy inhomogeneity and reduced interface roughness as suggested by HRXRD and AFM data. For the transition energy, we obtained relatively good agreement between experiment and simulations. Our results indicate that the ISBA of AlInN/GaN superlattices is comparable to that of the highest-quality AlN/GaN materials grown under optimal conditions at high temperature. Unexpectedly, the near-infrared integrated intensity of the heaviest doped samples exceeds theoretical calculations of a simplified model that assumes accuracy of structural parameters and considers barrier doping as the only free parameter. Further work is needed to elucidate Si activation energy in AlInN and to fully reproduce ISBA integrated intensity in AlInN/GaN superlattices.

We acknowledge support from the National Science Foundation. M.S.-HD and C.E. were supported by the NSF Award No. DMR-1206919. S.D., S.L., J.S., and O.M. acknowledge partial support from NSF Grant No. ECCS-1253720. This research also used resources of the Center for Functional Nanomaterials, which is a U.S. DOE Office of Science Facility, at Brookhaven National Laboratory under Contract No. DE-SC0012704.

[1]M. Beeler, E. Trichas, and E. Monroy, Semicond. Sci. Technol. **28**, 074022 (2013).
[2]D. Li, L. Tang, C. Edmunds, J. Shao, G. Gardner, M. J. Manfra, and O. Malis, Appl. Phys. Lett. **100**, 252105 (2012).
[3]C. Edmunds, J. Shao, M. Shirazi-HD, M. J. Manfra, and O. Malis, Appl. Phys. Lett. **105**, 021109 (2014).
[4]O. Mitrofanov, S. Schmult, M. J. Manfra, T. Siegrist, N. G. Weimann, A. M. Sergent, and R. J. Molnar, Appl. Phys. Lett. **88**, 171101 (2006).
[5]O. Malis, C. Edmunds, M. J. Manfra, and D. L. Sivco, Appl. Phys. Lett. **94**, 161111 (2009).
[6]C. Edmunds, L. Tang, D. Li, M. Cervantes, G. Gardner, T. Paskova, M. J. Manfra, and O. Malis, J. Electron. Mater. **41**, 881 (2012).
[7]C. Edmunds, L. Tang, J. Shao, D. Li, M. Cervantes, G. Gardner, D. N. Zakharov, M. J. Manfra, and O. Malis, Appl. Phys. Lett. **101**, 102104 (2012).
[8]C. Edmunds, L. Tang, M. Cervantes, M. Shirazi-HD, J. Shao, A. Grier, A. Valavanis, J. D. Cooper, D. Li, G. Gardner, D. N. Zakharov, Z. Ikonic, D. Indjin, P. Harrison, M. J. Manfra, and O. Malis, Phys. Rev. B **88**, 235306 (2013).
[9]L. Zhou, D. J. Smith, M. R. McCartney, D. S. Katzer, and D. F. Storm, Appl. Phys. Lett. **90**, 081917 (2007).
[10]S. Choi, F. Wu, R. Shivaraman, E. C. Young, and H. S. Speck, Appl. Phys. Lett. **100**, 232102 (2012).
[11]S. Fernández-Garrido, Ž. Gačević, and E. Calleja, Appl. Phys. Lett. **93**, 191907 (2008).
[12]S. W. Kaun, E. Ahmadi, B. Mazumder, F. Wu, E. C. H. Kyle, P. G. Burke, U. K. Mishra, and J. S. Speck, Semicond. Sci. Technol. **29**, 045011 (2014).
[13]M. T. Hardy, D. F. Storm, N. Nepal, D. S. Katzer, B. P. Downey, and D. J. Meyer, J. Cryst. Growth **425**, 119 (2015).
[14]S. Birner, T. Zibold, T. Andlauer, T. Kubis, M. Sabathil, A. Trellakis, and P. Vogl, IEEE Trans. Electron Devices **54**, 2137 (2007).
[15]R. Collazo, S. Mita, J. Xie, A. Rice, J. Tweedie, R. Dalmau, and Z. Sitar, Phys. Status Solidi C **8**, 2031 (2011).
[16]M. Tchernycheva, L. Nevou, L. Donyennette, F. H. Julien, E. Warde, F. Guilliot, E. Monroy, E. Bellet-Amalric, T. Remmele, and M. Albrecht, Phys. Rev. B **73**, 125347 (2006).
[17]M. A. Py, L. Lugani, Y. Taniyasu, J.-F. Carlin, and N. Grandjean, Phys. Rev. B **90**, 115208 (2014).
[18]Z. Chen, K. Fujita, J. Ichikawa, Y. Sakai, and T. Egawa, Jpn. J. Appl. Phys., Part 1 **50**, 081001 (2011).
[19]P. Ramvall, P. Riblet, S. Nomura, Y. Aoyagi, and S. Tanaka, J. Appl. Phys. **87**, 3883 (2000).
[20]A. Deteil, A. Vasanelli, Y. Todorov, C. Feuillet Palma, M. Renaudat St-Jean, G. Beaudoin, I. Sagnes, and C. Sirtori, Phys. Rev. Lett. **109**, 246808 (2012).